Granular Matter (2012) 14:63–69
DOI 10.1007/s10035-011-0297-9

ORIGINAL PAPER

Highly nonlinear solitary waves in chains of cylindrical particles

Devvrath Khatri · Duc Ngo · Chiara Daraio

Received: 19 May 2011 / Published online: 7 December 2011

Abstract We study the dynamic response of uniform granular chains composed of short cylindrical particles excited by an impulse. The particles in the chains are arranged with their axes orthogonal to the chain's axis, and the particles maintain a constant relative orientation angle. We study the formation and propagation of solitary waves in the chains varying the orientation angle (α) between particles, and show tunability of the stress transfer as a function of α. We use the general Hertzian contact theory to model the interaction between particles. We compare experimental findings with theoretical predictions based on the long wavelength approximation, and with numerical predictions based on a one-dimensional discrete particle model, and on a three-dimensional finite element approach, finding good agreement.

Keywords Highly nonlinear solitary waves · Finite element modeling · Granular materials · Cylindrical particles · Tunability

1 Introduction

In recent years, the study of the nonlinear dynamics of one-dimensional chains of spherical particles has received considerable attention [1–17]. Interest on these systems derives from their tunable dynamic response, encompassing linear, weakly nonlinear and strongly nonlinear regimes, controlled by varying the static and dynamic load applied [6,9,13]. In chains with a very weak (or zero) static precompression, the propagation of compressive pulses is strongly nonlinear, and it is characterized by the formation of stable solitary waves with a compact support, and with a speed of propagation dependent on the dynamic force amplitude [1,6]. The propagation properties of these waves can also be tuned by modifying the particle's dimension and material properties [2,6,9]. These tunable characteristics derive from the combination of nonlinearity of the particles' interaction (i.e., a power-law type contact potential in compression, and zero strength in tension), and of discreteness of the system. Chains of spherical particles have been proposed for many practical applications, such as shock and energy absorbing layers [7,8,18,19], sound focusing devices (tunable acoustic lenses) [20], and in non-destructive evaluation/structural health monitoring [21–24].

In this paper, we study the formation and propagation of nonlinear waves in a weakly compressed chain composed of uniform cylindrical particles arranged with their axes perpendicular to the chain's axis. In this case, the contact interaction between particles is a function of the relative orientation angle (α) between the particles' axes. This provides an additional design parameter for controlling the dynamic response of the system, compared to chains of spherical particles.

The remainder of this paper is organized as follows: In Sect. 2, we describe the experimental set up. In Sect. 3, we review the general Hertzian contact theory to describe the power law interaction between cylindrical particles under a non-conformal contact. In Sect. 4, we provide a theoretical description for highly nonlinear solitary wave's propagation in a uniform chain of cylindrical particles, based on long wavelength approximation and the Hertzian contact law. Sections 5 and 6 present our numerical approaches in support of the theory and the experimental findings: Sect. 5 introduces the discrete particle model and Sect. 6 the finite element model. In Sect. 7.1, we present the quasistatic validation (using a comparison with the Hertzian contact law) of our finite element simulations for the contact between two

D. Khatri · D. Ngo · C. Daraio (✉)
Engineering and Applied Science, California Institute of Technology, Pasadena, CA 91125, USA
e-mail: daraio@caltech.edu

cylindrical particles. In Sect. 7.2, we provide the experimental results for the propagation of compressive waves in a chain of cylindrical particles, and we compare the obtained results with the theoretical predictions and the numerical simulations. In this section, we also discuss the effect of different particle orientation on the wave propagation. The paper ends with conclusions and plans for future work in Sect. 8.

2 Experimental setup

The experimental setup used in this paper consisted of 20 stainless steel (316 type, from McMaster-Carr) cylindrical particles assembled in a vertical chain such that the orientation angle (α) between the axes of two adjacent cylinders is 90° (Fig. 1a). Each particle has a mass $m = 0.68\,\text{g}$; radius $R = 2.38\,\text{mm}$ and length $L = 4.76\,\text{mm}$ (Fig. 1b). The modulus of elasticity (E) of the particles is equal to 193 GPa and the Poisson's ratio (ν) is equal to 0.3 [25,26]. The chain of particles in the experiments was supported by guided rails consisting of four garolite rods. These rails ensured the unidirectional motion of the particles along the chain's axis. A single pulse was excited by impacting the chain with a stainless steel (316 type) spherical striker of comparable mass ($m = 0.45\,\text{g}$) to that of the cylindrical particles in the chain. To study the dependence of the propagating wave speed (V_s) on the amplitude of the dynamic force (F_m), we performed experiments varying the striker impact velocity (controlled by varying the drop-height of the striker).

We embedded piezo-sensors in selected particles in the chain for monitoring wave propagation along the chain. The assembly of the sensor particles was achieved following a procedure similar to the one described in [9] for spherical particles (Fig. 1c). These particles were connected to a Tektronix oscilloscope (TDS 2024) for data acquisition. For the measurements described in this paper, the sensors were placed in the 7th and 13th particles from the top of the chain. The sensor particles used in the experiments were pre-calibrated using conservation of momentum.

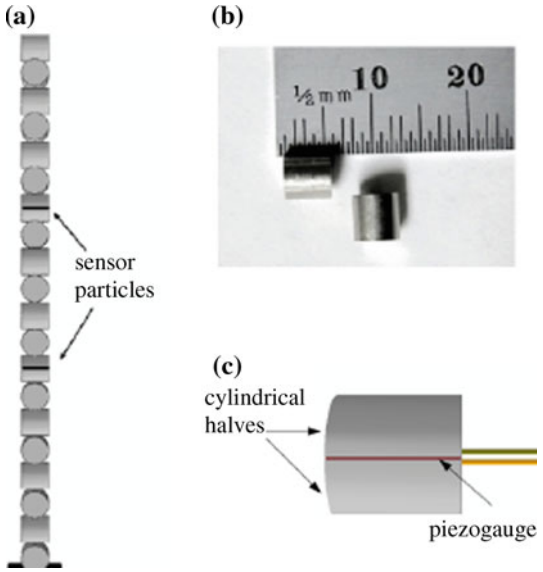

Fig. 1 (Color online) **a** Schematic diagram of the cylindrical particle's chain. The chain is composed of 20 elements, stacked vertically. Piezoelectric sensors were embedded in particles at location number 7 and 13. The orientation angle α between two adjacent particles in this setup is 90°. **b** Digital image showing the cylindrical particles used in the experiments. **c** Schematic diagram representing a sensor particle with embedded piezo-gauge

3 Contact interaction between two cylindrical particles

The contact area created by compressing two cylindrical surfaces against each other depends on the orientation angle (α) between the axes of the two cylinders. For small deformations, this could result in (i) a circular contact area ($\alpha = 90°$), (ii) an elliptical contact area ($0° < \alpha < 90°$), (iii) a very thin rectangular contact area ($\alpha = 0°$). For the first two cases, the contact interaction between two particles can be described by the Hertzian contact law which presented in [27] and briefly summarized here. Let δ denote the total displacement of two cylindrical particles under compression. The relation between the contact force F and the displacement δ can be obtained from [27] as:

$$F = \frac{4}{3}\frac{\sqrt{R_e}E^*}{F_2^{3/2}}\delta^{3/2} = k_{cyl}\delta^{3/2}, \tag{1}$$

where R_e is the equivalent radius and $R_e = R/sin\alpha$, the effective modulus E^* is defined as $E^* = \frac{E}{2(1-\nu^2)}$. The correction factor F_2 depends on the eccentricity of the elliptical contact area $\varepsilon = \sqrt{1-(b/a)^2}$ according to the following relation:

$$F_2 = \frac{2}{\pi}K(\varepsilon)\left\{\frac{4}{\pi\varepsilon^2}\sqrt{\left[\left(\frac{a}{b}\right)^2 E(\varepsilon) - K(\varepsilon)\right]\left[K(\varepsilon) - E(\varepsilon)\right]}\right\}^{-1/3}, \tag{2}$$

where $K(\varepsilon)$, $E(\varepsilon)$ are the complete elliptic integral of the first and second kind respectively, a is the semi-major and b is the semi-minor axes of the elliptical contact area, and $\frac{b}{a} \approx \left(\frac{1+\cos\alpha}{1-\cos\alpha}\right)^{-2/3}$. For the case $\alpha = 90°$, the correction factor F_2 equals to 1. Comparing this contact interaction with the contact interaction between two identical spherical particles $F = k_c\delta^{3/2}$ [27], with the contact stiffness $k_c = \frac{\sqrt{2R}E}{3(1-\nu^2)}$, it is important to notice that the contact stiffness of the cylindrical particles k_{cyl} depends on angle α, differently from the case of spherical particles.

The quasi-static contact model described above relies on the assumption that the semi-major axis a in the contact area

is much smaller than the particle's radius (R), to ensure each cylinder can be considered as an elastic half-space. At the same time, the ratio $\frac{b}{a}$ of the contact area shows a strong dependence on α, and when $\alpha \to 0°$, a becomes very large compared to b. In this case a can become larger than R, violating the assumption.

When $\alpha = 0°$, the two cylindrical particles are parallel to each other, reducing the contact area to a line. In this case, the Hertzian contact model mentioned above is invalid because R_e and F_2 are undefined. For two parallel cylindrical particles of the same radius, under a compressive force F^* (where F^* is force per unit length), the total displacement δ is given by [27]:

$$\delta = 2F^* \frac{1-\nu^2}{\pi E}\left[2ln\left(\frac{4R}{w}\right) - 1\right], \tag{3}$$

where $w = \sqrt{\frac{4F^*R(1-\nu^2)}{\pi E}}$ is the semi-contact width, which also depends on F^*. From Eq. 3, we can see that the line contact interaction is not a linear relation. The contact force in this case can be represented in terms of the total displacement as:

$$F^* = \frac{\pi E}{1-\nu^2}\left[\frac{\delta}{2}\frac{1}{W\left(-\frac{e\delta}{8R}\right)}\right] \tag{4}$$

where W is the Lambert function (or omega function), e is mathematical constant $e = 2.718$, and $x = W(y)$ is the solution of $xe^x = y$.

4 Wave propagation in a chain of cylindrical particles

A chain of spherical particles can be modeled as an array of rigid bodies (masses) connected by nonlinear springs, defined by the Hertzian contact law in compression and a zero tensile response. For this system, it is possible to write a discrete set of equations that describes the motion of the particles [1,6]. When the system is excited by a striker, the highly nonlinear dynamic response of the particles reveals the formation of compact solitary waves with unique properties. Starting from the discrete equations of motion for a weakly compressed chain of uniform spherical particles, and using a long wavelength approximation, Nesterenko derived a characteristic highly nonlinear wave equation that captures the fundamental properties of the system. The solution of the highly nonlinear wave equation describes the solitary wave shape and provides a nonlinear relation between wave amplitude and speed [1,6]. The solitary wave speed in chains of spherical particles was found to be a nonlinear function of the maximum dynamic contact force, and of the initial static compressive loading [9]. For a weakly compressed chain of uniform cylindrical particles in which $\alpha \neq 0°$, a similar procedure can be followed. The Hertzian contact interaction between two cylindrical particles has a power law formulation similar to the one between two spherical particles, differing only in the definition of the contact stiffness. Therefore, under the long wavelength approximation, we expect the weakly compressed chain of cylindrical particles to also support the formation and propagation of highly nonlinear solitary waves with properties similar to those of chains composed of spherical particles. Following [9], the analytical formulation describing the relation between the solitary wave speed V_s and the normalized force $f_r = F_m/F_0$ (F_m is the maximum dynamic contact force in the chain, and F_0 is the initial compressive force applied to the chain) can be obtained as:

$$V_s = D\sqrt{\frac{4k_{cyl}^{2/3}}{5m}}F_0^{1/6}\frac{1}{f_r^{2/3}-1}\left[\frac{3}{2} + f_r^{5/3} - \frac{5}{2}f_r^{2/3}\right]^{1/2} \tag{5}$$

where $D = 2R$ is the diameter of the cylindrical particles. Because the power law exponent n in the contact formulation is still $n = 1.5$ (as in the spherical particles case), the width of the propagating highly nonlinear solitary waves can also be expected to be ~5 times the particles' diameter.

For a weakly compressed chain of uniform cylindrical particles in which $\alpha = 0°$, a similar procedure cannot be followed because the contact interaction in this case is not a power law formulation as shown in Eq. 4. For very small values of orientation angle α the exponent n depends on α and it can deviate from the value 1.5. We discuss this case using numerical simulations in the following sections of this paper.

5 Discrete particle model (DPM)

We used a conventional discrete particle model (DPM) [9,14,28,29] to simulate the wave propagation in the chain of cylindrical particles. The cylindrical particles were considered as point masses connected with each other through nonlinear springs (Eqs. 1, 4), as the sound speed of elastic waves within the particles is much larger than the speed of propagation through the chain. We neglected all losses originating from internal resonance or friction. We used a fourth order Runge-Kutta method to solve the equations of motion of the system.

6 Finite element model (FEM)

We created a three-dimensional finite element model (FEM) for the chain of cylindrical particles. The model was generated in Abaqus/CAE and it was solved in Abaqus/Explicit. The cylindrical particles were modeled as solid (continuum) three-dimensional bodies, and they were meshed with tetrahedral elements of second order (using the modified 10-node tetrahedral elements C3D10M). The appropriate

mesh size for the particles was determined based on a mesh convergence study. The material and geometrical parameters of the cylindrical particles were obtained from the experimental setup described in Sect. 2. The end of the chain was modeled as a rigid wall composed of R3D3 elements. To model correctly the contact interaction between any two bodies (particle-particle, particle-wall) for quasi-static and dynamic problems, we used the Abaqus-Explicit surface-to-surface hard contact method. In this method, the primary surface in the contact pair is called the master surface and the secondary surface is called the slave surface. The surface-to-surface method uses the normal vector of the individual elements on the slave surface to match the normal vector of the individual elements on the master surface in order to determine the distance (gap or penetration) between the two surfaces. Once the slave surface generates contact with the master surface, the kinematic constraint applied on the contact pair uses the surface-to-surface method information along with hard-contact pressure-over closure to develop adequate force on the two contacting surfaces. This prevents penetration or overlap between the surfaces thereby maintaining the surface contact until the two bodies start moving apart. The hard-contact pressure-over closure model generates zero force when the two surfaces are not in contact. For simplicity, we modeled frictionless contact interaction in the tangential direction. The force calculated from the contact constraint model is the contact force between the two bodies. More information regarding the Abaqus's elements and contact interaction can be found in [30,31].

7 Results and discussion

7.1 Contact interaction between two cylindrical particles

We studied the quasi-static compression of two cylindrical particles (see Fig. 2a and b) to validate our finite element model and to verify the limits of validity for the contact interaction law described in Sect. 3, when the orientation angle α between two cylinders is small. We simulated the contact process between two particles having the same properties as the particles used in experiments, at different relative orientation angles α ($\alpha \in [0°, \ldots, 90°]$). We imposed a fixed maximum displacement δ between the two particles, such that δ is much smaller than the particle's diameter (to satisfy Hertz's small displacement assumption [27]).

The variation of contact force as a function of increased displacement between the two particles is plotted in Fig. 2c. Here we compare the response for selected orientation angles α, in the range of contact forces of interest for experiments. The Hertzian theoretical responses (see Sect. 3) are represented by the solid curves, while the results obtained from our FE simulations are represented by the dashed curves.

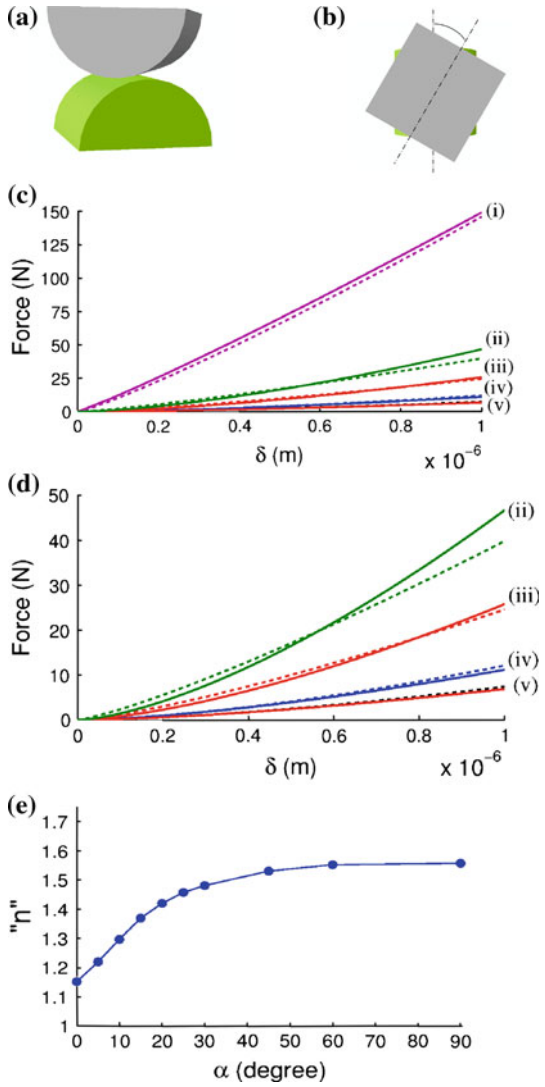

Fig. 2 (Color online) **a** Schematic diagram showing isometric view and **b** *top view* of two cylindrical particles in contact. **c** Comparison of the contact force-displacement relations obtained with the Hertzian contact model (*solid curves*), and with our finite element model (*dashed curves*). Results obtained for a contact between two cylindrical particles oriented at a relative angle $\alpha = 0°$ (curve group *(i)*), $\alpha = 5°$ (curve group *(ii)*), $\alpha = 10°$ (curve group *(iii)*), $\alpha = 30°$ (curve group *(iv)*) and $\alpha = 90°$ (curve group *(v)*). **d** Detailed view of (**c**) for $\alpha = 5°, 10°, 30°, \& 90°$. **e** Dependence of the exponent n in a generic power-law type contact interaction between two cylindrical particles on the orientation angle α, obtained from finite element analysis

For large orientation angles α, we observed good agreement between theory and numerical results. When the orientation angle α decreases, i.e. $\alpha \to 0°$, the violation of assumptions used in the theoretical model leads to an evident discrepancy between the curves (see Fig. 2c and d).

To study the evolution of the contact response between two cylinders with variations of the angle α, we assumed that the contact interaction between two identical particles can always be expressed in the form of a generalized power-law, as:

$$F = k_{cyl}\,(\alpha)\,\delta^{n(\alpha)} \tag{6}$$

We used this power law to fit results obtained with our finite element model (Fig. 2d) and plot the values of the exponent n as a function of α (Fig. 2e). For $\alpha > 30°$ the value of n is close to 1.5 which is as expected from the Hertzian contact theory, while for smaller angles $0° < \alpha < 30°$ the exponent n deviates from 1.5, and gradually decreases as the angle decreases. When $\alpha = 0°$, we have a line contact between the two interacting cylinders. For this case, if the contact interaction is approximated by a power law formulation, we obtain the power-law exponent value $n = 1.15$ which is close to the value 1.11 reported in [32].

7.2 Dynamic response of a chain of cylindrical particles

We tested experimentally the dynamic response of a vertically aligned, one-dimensional chain composed of 20 uniform cylindrical particles with relative orientation angle $\alpha = 90°$, excited by a stainless steel spherical striker of mass $m = 0.45\,\text{g}$, with an impact velocity $v = 0.5\,\text{m/s}$. The force profiles measured in time by the sensors positioned at particle number 7 and 13 are shown in Fig. 3a. We compared the experimental data with numerical results obtained with the discrete particle model based on Hertzian contact interactions, and with the three-dimensional FE model, finding very good agreement between them (Fig. 3a). We calculated the wave speed by dividing the distance of the two sensors with the time taken for the peak of the wave to travel between them. The solitary wave speed obtained from the finite element model, discrete particle model, and experiments were 539.2, 544 m/s, and 559 ± 28 m/s, respectively. The width of the propagating pulses was measured to be 6 particle diameter from experimental data, which is close to the 5 particle size of solitary wave's reported in earlier studies for chains of spherical particles [1,6].

We studied the relation between wave speed and maximum dynamic contact force in Fig. 3b. It should be noted that the force measured by the sensors in our experiments is the average of the two dynamic forces at the contacts with the adjacent particles [28]. To compare experiments with our discrete numerical simulations we obtained the maximum dynamic contact force in experiments $\left(F_{m,exp}\right)$ following the procedure reported in [28]. We calculated numerically the coefficient β as the ratio between the maximum contact force and the maximum average force in a given particle (the instrumented particle in our case), $\beta = \frac{F_{m,num}}{F_{avg,num}}$. The maximum dynamic contact force $F_{m,exp}$ can then be calculated as $F_{m,exp} = \beta F_{avg,exp}$, where $F_{avg,exp}$ is the force measured by the sensors in our experiments. From Fig. 3b, it is evident that the experimental and numerical results are in good agreement, demonstrating the formation and propagation of highly nonlinear solitary waves. Similarly to what reported

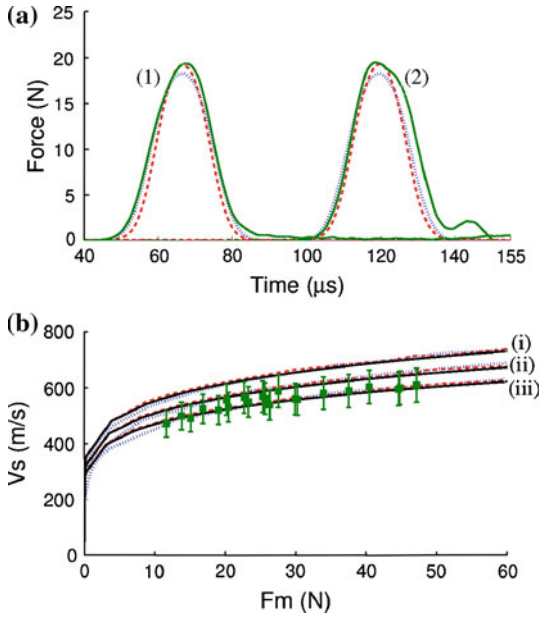

Fig. 3 (Color online) **a** Comparison of experimental and numerical results, obtained from the finite element and the discrete particle model, for the wave propagation in a chain of cylindrical particles with orientation angle $\alpha = 90°$. The curve groups (*1*) and (*2*) are results obtained from the instrumented particles placed at location number 7 and 13 from the top of the chain, respectively. The *solid curves* represent experimental data. The *dashed curves* are obtained from our discrete particles model, and the *dotted curves* from FEM. **b** Dependence of solitary wave speed on the maximum dynamic contact force in the chain of cylindrical particles when $\alpha = 30°$ (curve group *(i)*), when $\alpha = 45°$ (curve group *(ii)*), and when $\alpha = 90°$ (curve group *(iii)*). Experimental data are reported only for $\alpha = 90°$, and it is shown by *solid squares*. The theoretical results for all the angles in each group are shown by *solid curves*. The results obtained with our discrete particle model are represented by the *dashed curve* and the finite element results are represented by the *dotted curves* in each group

for chains of spherical beads [6,9,13], the dynamic response of chains of cylindrical particles can be tuned by varying the radius and/or the material properties of the particles, the initial precompression, and dynamic force applied to the system. However, the cylindrical geometry of the particles offers an additional parameter for tunability: the orientation angle between consecutive cylinders.

We studied numerically the effect of particle orientation on the wave propagation in the system. Figure 3b shows the variation of wave speed as a function of dynamic force for selected values of $\alpha = [30°, 45°, 90°]$. For a particular orientation angle α, the dynamic force is varied by changing the striker impact velocity. As the α value decreases the contact stiffness k_{cyl} increases (Eq. 1) which results in higher wave speeds for the same dynamic load (Eq. 5). For example, when the orientation angle between cylindrical particles was $\alpha = 90°$, for the dynamic load of $F_m = 40\,\text{N}$, the wave speed was $V_s = 591.3\,\text{m/s}$. When the orientation angle was

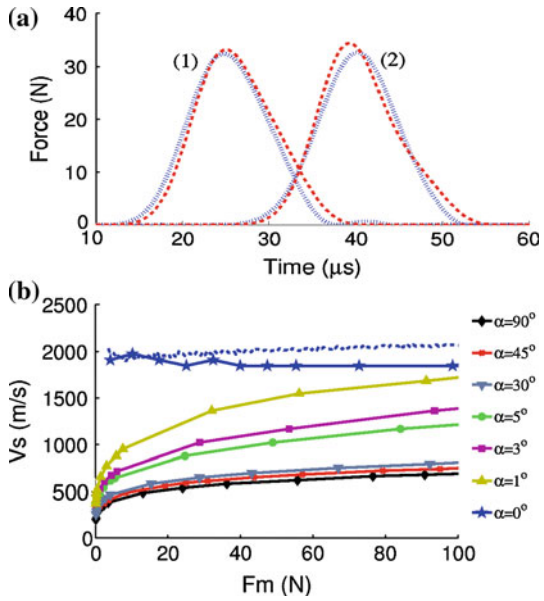

Fig. 4 (Color online) Numerical results showing the dynamic response of a chain composed of parallel cylinders ($\alpha = 0°$). **a** Force profiles in time obtained for a wave traveling in a chain of parallel particles using our finite element model (*dotted curves*), and our discrete particles model (*dashed curves*). The curve groups (*1*) and (*2*) represent results obtained for the waves traveling through the 7th and 13th particles from the top of the chain. **b** Dependence of wave speed on the maximum dynamic contact force. The *solid lines* represent results obtained with our FEM for different values of the relative orientation angle $\alpha = [0°, 1°, 3°, 5°, 30°, 45°, 90°]$. The *dotted line*, shown for $\alpha = 0°$, reports data obtained with the DPM

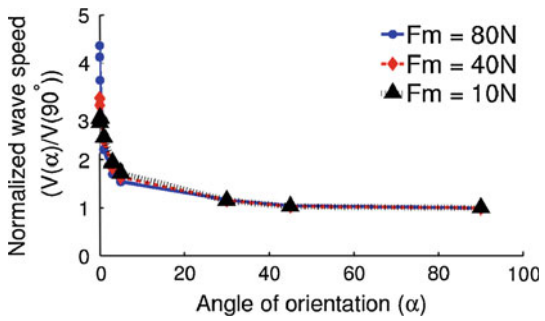

Fig. 5 (Color online) FEM results showing the dependence of the wave speed (normalized with respect to the wave speed in the case $\alpha = 90°$) as a function of the orientation angle α. The three curves correspond to 3 different dynamic force values, the *solid curve* with circular markers is for $\boldsymbol{F_m} = 80\,\mathrm{N}$, the *dashed curve* with diamond markers corresponds to $F_m = 40\,\mathrm{N}$ and the *dotted curve* with triangular markers is for $\boldsymbol{F_m} = 10\,\mathrm{N}$

lower than $\alpha = 90°$ the wave speed increases. The speed is 9% higher for $\alpha = 45°$ and 16% higher for $\alpha = 30°$.

The case $\alpha = 0°$ (Fig. 4) presented unique features: The shape of the propagating waves is significantly different from the cases for which $\alpha > 0°$. The width of these waves, for an impulse generated by a striker of mass $m = 0.45\,\mathrm{g}$ with velocity 0.5 m/s, is ∼10 particle diameters (see Fig. 4). The wave speed is ∼4 times the value observed for other cases, and does not appear to change significantly in the range of dynamic force considered (see Fig. 4b). This interesting behavior for $\alpha = 0°$ originates from the fact that the contact interaction does not have a power-law type relation (see Sect. 3).

Using FEM, we also studied the sensitivity of the system towards the small angle variation near $\alpha = 0°$ (Fig. 4b). From the FEM results, we found that the dynamic response of this system is very sensitive to the change of the orientation angle, i.e., the wave speed changes significantly with small changes in the value of α. Because of the imperfect nature of the experimental setup (e.g., the non-uniformity of the particles, especially the sensor particles, and the tolerances between the particles and the support system) the measurements of the wave propagation in a chain of cylinders with small α presented significant variability. From the FEM analysis and discrete particle simulations, we found that the wave speed in the chain of cylindrical particles increases dramatically as the orientation angle decreases, for a given dynamic force (the solid curve with star markers and the dotted curve in Fig. 4b represent results obtained with the FEM and the DPM, respectively). The angle of orientation has a significant effect on the solitary wave speed as $\alpha \to 0°$. In Fig. 5 we calculated the normalized solitary wave speed (with respect to the wave speed in case of $\alpha = 90°$) as a function of α for selected values of dynamic force. From this figure it appears clear that in the range of small α ($0° < \alpha < 10°$) the wave speed changes significantly with small changes of α, while in the range of large values of α, the wave speed is not very sensitive to the changes of angle of orientation.

In recent studies we have also found that the length of the cylindrical particles has an important effect on the wave propagation in the system. As the length of the cylinders increases, more energy from the initial impulse is transfered to vibrational modes of individual particles. The effects of the vibrational properties of the particles in the wave propagation are currently being investigated.

8 Conclusions

We studied the wave propagation in a chain composed of uniform cylindrical particles with axes perpendicular to the chain's axis. The particles were arranged such that the orientation angle α between the axes of neighboring particles is uniform throughout the chain. We reviewed the Hertzian contact interaction between two cylindrical particles and its dependence on the orientation angle α. We compared results from the Hertzian contact law with a three-dimensional finite element model to find the range of α in which the Hertzian contact law is valid. We used the contact interaction between

particles in a discrete particle model, to study the properties of wave propagation. We observed the formation and propagation of highly nonlinear solitary waves, similar to the uniform chain of spherical particles, when $\alpha > 0°$, with good agreement between the discrete particle and finite element models. We compared the numerical results with experiments for the case of $\alpha = 90°$. We analyzed the dynamic response of the system with variations of the angle α and showed that the response of the system is tunable with α. Chains of cylindrical particles could find application in the design of materials capable of tailoring stress wave propagation, and in tunable acoustic devices.

Acknowledgments We thank Mr. Ivan Szelengowicz for performing preliminary experiments. The authors acknowledge support from the Army Research Office (MURI), Dr. David Stepp is the grant monitor, and from the National Science Foundation (Grant Numbers 825345, 844540).

References

1. Nesterenko, V.: Propagation of nonlinear compression pulses in granular media. J. Appl. Mech. Tech. **5**, 733–743 (1983)
2. Coste, C., Falcon, E., Fauve, S.: Solitary waves in a chain of beads under Hertz contact. Phys. Rev. E **56**, 6104–6117 (1997)
3. Sen, S., Manciu, M.: Discrete Hertzian chains and solitons. Phys. A Stat. Mech. Appl. **268**(3), 644–649 (1999)
4. Chatterjee, A.: Asymptotic solution for solitary waves in a chain of elastic spheres. Phys. Rev. E **59**(5), 5912–5919 (1999)
5. Hascoët, E., Herrmann, H.J., Loreto, V.: Shock propagation in a granular chain. Phys. Rev. E **59**(3), 3202–3206 (1999)
6. Nesterenko, V.: Dynamics of Heterogeneous Materials. Springer, New York (2001)
7. Hong, J.: Universal power-law decay of the impulse energy in granular protectors. Phys. Rev. Lett. **94**(108001), 1–4 (2005)
8. Doney, R., Sen, S.: Decorated, tapered, and highly nonlinear granular chain. Phys. Rev. Lett. **97**(155502), 1–4 (2006)
9. Daraio, C., Nesterenko, V., Herbold, E., Jin, S.: Strongly nonlinear waves in a chain of polymer coated steel beads. Phys. Rev. E **73**(026612), 1–7 (2006)
10. Vergara, L.: Delayed scattering of solitary waves from interfaces in a granular container. Phys. Rev. **73**(066623), 1–4 (2006)
11. Herbold, E.B., Nesterenko, V.F.: Shock wave structure in a strongly nonlinear lattice with viscous dissipation. Phys. Rev. E **75** (021304), 1–8 (2007)
12. Rosas, A., Romero, A.H., Nesterenko, V.F., Lindenberg, K.: Observation of two-wave structure in strongly nonlinear dissipative granular chains. Phys. Rev. Lett. **98**(164301), 1–4 (2007)
13. Sen, S., Hong, J., Bang, J., Avalos, E., Doney, R.: Solitary waves in the granular chain. Phys. Rep. **462**(2), 21–66 (2008)
14. Porter, M., Daraio, C., Herbold, E., Szelengowicz, I., Kevrekidis, P.: Highly nonlinear solitary waves in phononic crystal dimmers. Phys. Rev. E **77**(015601(R)), 1–4 (2008)
15. Job, S., Santibanez, F., Tapia, F., Melo, F.: Wave localization in strongly nonlinear Hertzian chains with mass defect. Phys. Rev. E **80**(025602), 1–4 (2009)
16. Harbola, U., Rosas, A., Romero, A.H., Esposito, M., Lindenberg, K.: Pulse propagation in decorated granular chains: an analytical approach. Phys. Rev. E **80**(051302), 1–9 (2009)
17. Carretero, R., Khatri, D., Porter, M., Kevrekidis, P., Daraio, C.: Dissipative solitary waves in periodic granular media. Phys. Rev. Lett. **102**(024102), 1–4 (2009)
18. Daraio, C., Nesterenko, V., Herbold, E., Jin, S.: Energy trapping and shock disintegration in a composite granular medium. Phys. Rev. E **96**(058002), 1–4 (2006)
19. Fraternali, F., Porter, M.A., Daraio, C.: Optimal design of composite granular protectors. Mech. Adv. Mater. Struct. **17**, 1–19 (2010)
20. Spadoni, A., Daraio, C.: Generation and control of sound bullets with a nonlinear acoustic lens. Proc. Natl. Acad. Sci. USA **107**(7230), 1–5 (2010)
21. Sen, S., Manciu, M., Wright, J.D.: Soliton-like pulses in perturbed and driven hertzian chains and their possible applications in detecting buried impurities. Phys. Rev. E **57**, 2386–2397 (1998)
22. Hong, J., Xu, A.: Nondestructive identification of impurities in granular medium. Appl. Phys. Lett. **81**, 4868–4870 (2002)
23. Khatri, D., Daraio, C., Rizzo, P.: Coupling of highly nonlinear waves with linear elastic media. SPIE **7292**(72920), 1–9 (2009)
24. Yang, J., Silvestro, C., Khatri, D., Nardo, L.D., Daraio, C.: Interaction of highly nonlinear solitary waves with linear elastic media. Phys. Rev. E **83**(046606), 1–12 (2011)
25. Steel-AISI Type 316. Efunda Inc. http://www.efunda.com. Accessed 1 Aug 2010 (2011)
26. Bauccio, M.: ASM Metals Reference Book. 3rd edn. American Society for Metals, Materials Park, OH (1993)
27. Johnson, K.L.: Contact Mechanics. Cambridge University Press, Cambridge (1987)
28. Daraio, C., Nesterenko, V., Herbold, E., Jin, S.: Strongly nonlinear waves in a chain of teflon beads. Phys. Rev. E **72**(016603), 1–9 (2005)
29. Porter, M., Daraio, C., Szelengowicz, I., Herbold, E., Kevrekidis, P.: Highly nonlinear solitary waves in heterogeneous periodic granular media. Phys. D Nonlinear Phenom. **238**, 666–676 (2009)
30. Abaqus Documentation version 6.8. Simulia Dassault Systemes, S.A. Providence, RI. http://www.simulia.com/ (2008)
31. Khatri, D., Daraio, C.: Finite element model of the dynamic behavior of highly nonlinear granular chains. Finite. Elem. Anal. Des. (Submitted, 2011)
32. Harris, T.: Rolling Bearing Analysis. Wiley, New York (2001)